J Mater Sci (2009) 44:5673–5681
DOI 10.1007/s10853-009-3799-7

# Oxidation resistance of hafnium diboride—silicon carbide from 1400 to 2000 °C

**Carmen M. Carney**

Received: 1 April 2009 / Accepted: 5 August 2009 / Published online: 18 August 2009


**Abstract** Oxidation resistance tests were carried out on $HfB_2$-20 vol.% SiC prepared by spark plasma sintering. The dense samples were exposed from 1400 to 2000 °C in an ambient atmosphere for 1 h. For comparison, the same material was tested using an arc jet to simulate an atmospheric reentry environment. The oxidation properties of the samples were determined by measuring the weight gain per unit surface area and the thicknesses of the oxide scale. The oxide scale consists of a $SiO_2$ outer layer, porous $HfO_2$ layers, and an $HfB_2$ layer depleted in SiC. A transition in $HfO_2$ morphology from equixed to columnar and a decrease in $SiO_2$ viscosity between 1800 and 1900 °C accompanied a rapid increase in weight gain and scale thickness.

## Introduction

Due to their high melting temperatures, transition metal diborides such as $ZrB_2$ and $HfB_2$ commonly referred to as ultra high-temperature ceramics (UHTCs) are being considered as candidates for leading edges of sharp-bodied reentry vehicles [1–3]. While $ZrB_2$-based UHTCs have received a majority of the attention because of their lower density (6.09 vs. 10.5 g/cm$^3$ for $HfB_2$) and lower cost, $HfB_2$-based materials have been shown to be more oxidation resistant [4–6]. When $HfB_2$ is exposed to air at elevated temperatures, $HfO_2$ and $B_2O_3$ are formed. The $HfO_2$ scale is porous and the $B_2O_3$ evaporation limits the use of temperatures because of its 450 °C melting point [7] and high vaporization pressure. For protection at higher temperatures, $HfB_2$ is commonly mixed with SiC. The addition of SiC allows the formation of $SiO_2$ at elevated temperatures (>1100 °C). The $SiO_2$ reacts with $B_2O_3$ forming a borosilicate glass. After a series of studies in the late 1960s, the most commonly tested samples are $HfB_2$ with 10–30 vol.% SiC [2, 8]. Most evaluations of UHTC samples reported in the literature are limited to a maximum of 1630 °C by the air furnaces commonly used [2, 8–10]. It is not known if the $SiO_2$ offers sufficient protection at temperatures above 1630 °C, given that its melting point is 1713 °C [7]. For these materials to be used as leading edge materials on hypersonic aircraft they must be able to withstand temperatures up to 2000 °C in a reentry environment.

Oxidation at the lower temperatures (<1630 °C) produces a layered oxide scale consisting of a $SiO_2$-rich outer layer, a porous $HfO_2$ layer (with and without partially oxidized SiC), and the non-oxidized bulk. Some reports have shown the oxidation of $HfB_2$–SiC at higher temperatures such as ~1997 °C [8], but these reports do not compare similar samples tested at lower temperatures. Additionally, arc jet testing has been used to test $HfB_2$–SiC at temperatures up to and above 2000 °C [2, 11, 12]. At temperatures above 2200 °C in the arc jet, the $SiO_2$ is completely removed and only an $HfO_2$ scale remains. While arc jet testing is considered the most representative simulation of the conditions of hypersonic flight, the tests are limited in duration (usually ~1 min), and are expensive. Typically materials that perform well under low temperatures (<1630 °C) in an air furnace do not necessarily perform well in arc jet conditions. It is therefore

C. M. Carney
Air Force Research Laboratory, Materials and Manufacturing Directorate, AFRL/RX, Dayton, OH, USA

C. M. Carney (✉)
UES, Inc., Dayton, OH 45432, USA
e-mail: ccarney@ues.com

necessary to utilize a test method such as high-temperature furnace oxidation to properly evaluate materials prior to expensive arc jet testing, and to study long-term oxidation behavior. In this study, the oxidation behavior of $HfB_2$-20 vol.% SiC (hereafter $HfB_2$–SiC) is studied during isothermal exposures at temperatures of 1400 to 2000 °C, (a) to evaluate their behavior at temperatures greater than 1630 °C, (b) to compare them with data/behavior reported in the literature at temperatures below 1630 °C, and (c) to compare them with behavior during arc jet testing. Weight gain per surface area data are used as the measure of oxidation resistance. Scanning electron microscopy and X-ray diffraction analysis of the oxide scale are used to gain insight on the characteristics of the scale after exposure to high-temperature regimes.

## Experimental procedure

$HfB_2$ (Cerac, Milwaukee Wisconsin) and SiC (Reade Advanced Materials, East Providence Rhode Island) were used to mix 80-vol.% $HfB_2$ and 20-vol.% SiC. The $\beta$-SiC was 45–55 nm powder (reported) with 97.5% purity. The $HfB_2$ had a mean particle size of 4.6 μm (measured) and 99.5% purity. Powders were ball milled using $Si_3N_4$ grinding media in isopropanol for 18 h. The powders were then dried at room temperature while stirring followed by 18 h of dry milling with the same $Si_3N_4$. The weight loss of the $Si_3N_4$ grinding media was 0.1 wt% based on the total powder weight. The powder was sieved through an 80-mesh screen before sintering.

A total of 170 g of the dried powder were loaded into a 40-mm graphite die coated with BN and lined with graphite foil. The sample was sintered using spark plasma sintering (SPS: FCT Systeme GmbH Model HPD 25-1, Rauenstein, Germany) with a heating and cooling rate of 50 °C/min and a maximum temperature of 2100 °C (achieved using 6 V and 3.4 kA). The hold time was 17 mins. The temperature was measured by an optical pyrometer focused on the bottom of a bore hole in the punch ~5 mm from the powder. A vacuum of 150 Pa was maintained for the entire heating cycle. A DC current with a pulse sequence of 10 ms on and 5 ms off with a single pulse was used for heating. A uniaxial load of 32 MPa was applied on the heat up to 1600 °C and held during the remaining heating cycle.

A 25.4-mm diameter flat-faced model was cut from the sintered puck for arc jet testing using rotational electrical discharge machining (EDM). The geometry of the samples was dictated by the advanced heating facility (AHF) arc jet at NASA Ames [11]. The face of the sample was polished to 1 μm to remove oxidation caused by EDM machining and provide consistent starting surface finishes. From the remaining puck, 4-mm × 2.5-mm × 2-mm samples were cut using a diamond saw and polished on all sides to a 1-μm finish for oxidation tests.

$HfB_2$–SiC specimens were exposed to air at temperatures every 100 °C between 1400 and 1600 °C for 1 h using a horizontal $MoSi_2$ resistance heated tube furnace. Samples were also heated every 100 °C between 1600 and 2000 °C using a $ZrO_2$ element furnace (ZrF-25: Shinagawa Refractories Co., Tokyo Japan). The heating and cooling rates used for both furnaces were 5 °C/min. The heating rate was limited by the zirconia heating element. All the samples were placed on a zirconia crucible so that the two sides with the largest surface area were parallel to the zirconia crucible. The zirconia crucibles were concave such that the samples only made two line contacts along their corners with the crucible. Both the sample and the zirconia crucible weights were measured before and after oxidation using a balance with 0.01-mg precision. At least two samples were tested at each temperature.

The flat-faced models were exposed to sustained enthalpy flows using the AHF arc jet at NASA Ames. The main air mass flow rate during the test was 80 g/s and the stagnation pressure was 0.1 atm. The specimens were located at a distance of 6 cm from the exit nozzle. The cold-wall heat flux as measured using a copper slug 102-mm diameter hemisphere calorimeter was 260 W/cm$^2$. This resulted in a surface temperature between 1450 and 1570 °C for 3.6 min as measured by the three pyrometers. A 4-mm × 2.5-mm × 2-mm rectangular sample was heated in the furnace by pushing the sample into and out of the heated furnace within approximately 1 min and holding the sample at 1500 °C for 4 min to provide a comparison with the arc jet sample.

The microstructures of the as sintered and oxidized samples were studied by polishing the samples to a 1-μm finish. The furnace-heated samples were polished perpendicular to the top and bottom faces, where the top face was defined as exposed surface and the bottom face was the surface facing the zirconia crucible. The arc jet sample was cut with a diamond-loaded saw blade approximately 9 mm from the center of the sample and polished perpendicular to the exposed surface. The microstructures were characterized using SEM (Quanta, FEI, Hillsborough OR) along with energy dispersive spectroscopy (EDS: Pegasus 4000, EDAX, Mahwah NJ) for chemical analysis. The crystallography analysis of the oxide was performed on an X-ray diffractometer with Cu $K_\alpha$ radiation (XRD: Rigaku 2500, Tokyo Japan). The density of the samples was measured using the Archimedes method and He pycnometry (Accupyc 1330, Micromeritics, Norcross, GA). The reported density values are an average of seven measurements.

## Results

### Microstructure

He pycnometry analysis of the unprocessed $HfB_2$–SiC powder showed a density of 9.28 g $cm^3$. The sintered $HfB_2$–SiC sample was found to have a density of 9.23 g $cm^3$ by the Archimedes' test method and 9.24 g $cm^3$ by He pycnometry. The agreement between the He pycnometry and Archimedes' values suggest no open porosity in the sample as expected and the individual values both give a density over 99%. Figure 1 shows a SEM micrograph of the polished surface. Although some SiC grain pullout was observed to occur during polishing, the microstructure is regular with negligible residual porosity. The SiC, dark features, in Fig. 1 is homogeneously dispersed inter-granularly within the $HfB_2$ matrix. The individual SiC grains within the $HfB_2$ matrix are on the order of 2–3 μm in diameter.

### Weight gain due to oxidation (furnace heating)

The average weight gain per surface area as a function of temperature is plotted in Fig. 2a. The total weight gain was calculated by weighing both the sample and the zirconia crucible before and after the heating cycle and adding the two weight-change values. The samples heated in the $MoSi_2$ element tube furnace are plotted with the samples heated in the $ZrO_2$ element furnace. Samples were heated at 1600 °C in both furnaces for comparison. The values are within 0.2 mg/$cm^2$. Two samples were heated at each temperature. Only a small weight gain of 1.5 and 2.5 mg/$cm^2$ is observed at 1400 and 1500 C, respectively. The weight gain per surface area at 1600 and 1700 °C increases less than 0.5 mg/$cm^2$ over the 1500 °C value. The weight gain at 1900 °C more than doubles over the 1700 °C value. Literature values for weight gain during oxidation in air for $HfB_2$-20 vol.% SiC without sintering aids are rare. From Opila et al. [6] the weight gain was calculated from the provided rate constant to be 1.6 mg/$cm^2$ for samples held at 1627 °C for 1 h. This value is lower than the values found in this study, but the use of slower heating rates effectively increases the time at oxidizing temperatures compared to the literature values. Licheri et al. [13] heated $HfB_2$-26.5 vol.% SiC to 1450 °C at 2 °C/min and found

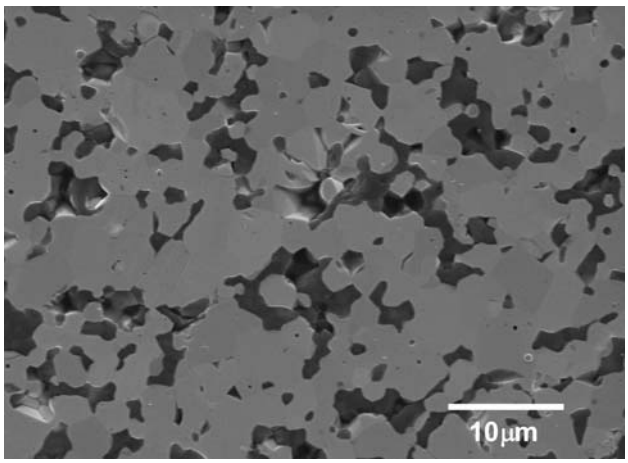


**Fig. 1** SEM micrograph showing the microstructure of the as sintered $HfB_2$–SiC sample. Some SiC grain pullout occurs during polishing

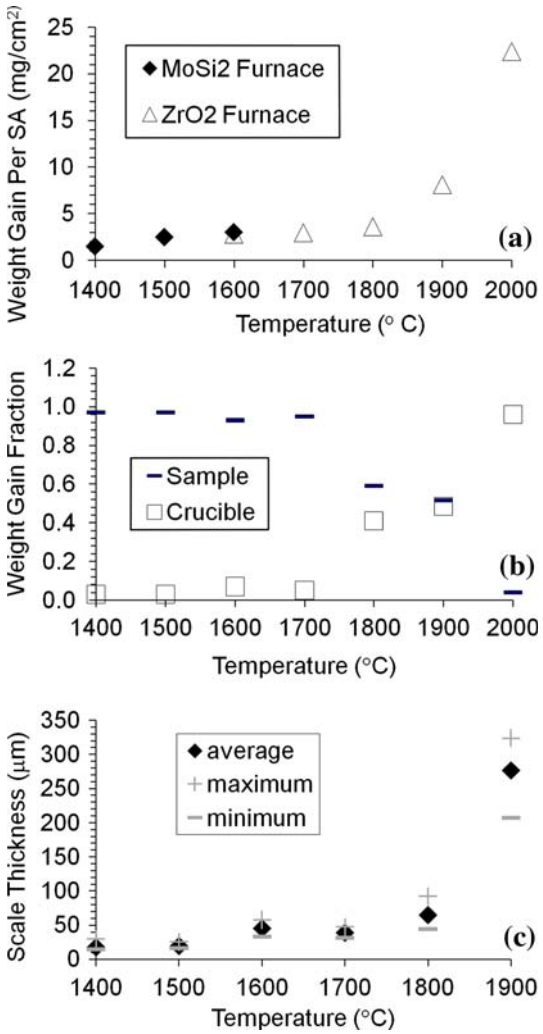


**Fig. 2** **a** Weight gain per surface area as a function of temperature for the $MoSi_2$ furnace-heated samples (*filled diamond*) and the $ZrO_2$ furnace-heated samples (*open square*). **b** The fraction of total weight gain that was measured for the sample (−) and the crucible (*open square*), the weight gain measured for the crucible resulted from $SiO_2$ flow onto the substrate. **c** The thickness of the oxide scale formed on the $HfB_2$–SiC after exposure was measured in at least 12 places along the top (as defined in the text) of the sample and the average (*filled diamond*), minimum (−), and maximum (+) values are plotted with respect to temperature

approximately 0.5-mg/cm$^2$ weight gain upon heating and 0.5-mg/cm$^2$ weight gain after a 1-h hold. Assuming a similar weight gain during cooling, the values are comparable with the data presented.

Post-oxidation observations suggested that some of the glass had flowed onto the zirconia crucible. To determine the degree of glass flow, the sample and the zirconia crucible were weighed individually, except for one of the samples heated to 2000 °C where the sample adhered to the crucible after heating. Figure 2b shows the fraction of the overall weight gain attributable to the sample and to the zirconia crucible. Since the zirconia crucible when heated alone did not show any weight gain at these temperatures, the change in weight of the crucible is attributed to the glass flow from the sample onto the crucible as observed after oxidation. Between 1400 and 1700 °C the sample was responsible for 95% or greater of the total weight gain. The weight change of the zirconia crucible was responsible for a majority of the weight change starting at 1800 °C (61%) and by 2000 °C accounted for 96% of the weight gain.

The thickness of the total oxide scale is shown in Fig. 2c for all the temperatures except 2000 °C where the entire $HfB_2$–SiC sample was oxidized. The total oxide scale is taken to be any region of the sample that has been affected by oxygen interaction. The maximum and minimum thicknesses measured are recorded along with the average thickness to show the variation in the scale thickness. For consistency, all the measurements were made on the top surface of the sample far enough away from the corners so that the more rapid oxidation that occurs there did not influence the results. At least 12 separate measurements were averaged for each sample. The scale thickness is less than 20-μm below 1500 °C and increases to 65 μm at 1800 °C.

## Oxide scale morphology (furnace heating)

SEM micrographs of the samples heated between 1400 and 2000 °C in the static air furnaces for 1 h are depicted in Fig. 3a–h. In general, four layers are defined (as shown in Fig. 3a–g) that will be used in the discussion. The layers in each sample were identified by EDS analysis of the dark (Si containing) and light (Hf containing) phases throughout the entire oxide scale. Layer I, the topmost layer, consists of primarily Si and O (presumably amorphous $SiO_2$). $B_2O_3$ has also been observed in this layer up to 1550 °C [5], but this was not tracked in this study. Layer II consists of a lighter phase containing O and Hf, and a darker phase containing O and Si which was interpreted as $SiO_2$ infiltrating porous $HfO_2$. Layer III is predominantly Hf and O (likely as $HfO_2$) and Layer IV is predominately $HfB_2$. Not all the four layers are formed at each temperature. Their thicknesses (Fig. 2c) and morphology (Fig. 3) were tracked with temperature to describe the evolution of the oxide scale with temperature. The following paragraphs describe the evolution of the layers.

Layer I ($SiO_2$) does not completely cover the surface of the sample until 1600 °C. At 1600 °C the glassy layer is between 10 and 20 μm in thickness. The layer grows with increasing temperature until it reaches a maximum at 1900 °C (greater than 100 μm in some locations). At 2000 °C the $SiO_2$ thickness is less than 30 μm. Bubbles form in the glassy layer starting at 1500 °C and have a dramatic impact on the morphology of the $SiO_2$ layer at 1900 °C as seen in Fig. 3f. Additionally, grains shown to contain Hf and O by EDS can be found in the $SiO_2$ layer as low as 1400 °C and become more frequent at higher temperatures.

Layer II (porous $HfO_2$ filled by $SiO_2$) is nondescript at 1400 and 1500 °C. At these temperatures the $SiO_2$ sits on top of the sample or only penetrates between voids at the surface, but reaches no further than one or two $HfO_2$ grain thicknesses. The layer develops to about 10 μm at 1600 °C and increases in thickness at 1700 °C. At 1800 °C the morphology of the layer begins to change. Instead of equiaxed $HfO_2$ grains that retain the original $HfB_2$ microstructure, the grains appear more columnar and the $SiO_2$ fills a thicker porous $HfO_2$ scale at 1900 °C. At 2000 °C the $HfO_2$ is distinctively columnar and Layer II has grown to around 300 μm.

Layer III, the predominantly $HfO_2$ layer, exists between 1400 and 1700 °C. At 1400 and 1500 °C it comprises the bulk of the oxide scale (20–30 μm) lying just below the $SiO_2$ layer. At these temperatures the layer consists of $HfO_2$ with inclusions of Si, C, and O as shown by EDS. The inclusions have varying concentrations of Si, C, and O and thus will be referred to as Si–O–C. The inclusions reside in the voids between the $HfO_2$ that are the same size and morphology as the SiC grains within the bulk suggesting that they are partially oxidized SiC. At 1600 and 1700 °C Layer III is located below the layer of $HfO_2$ filled by $SiO_2$ and does not grow much more than 5 μm. Si–O–C inclusions are also observed in Layer II at 1600 and 1700 °C. Although the samples presented here are mounted in a C-containing epoxy, sister samples were polished using a tripod polisher with no epoxy and the same Si–O–C inclusions are found. The same Si–O–C inclusions were found by the author when studying $ZrB_2$–SiC samples [14] and similar Si–O–C inclusions have been described in other $ZrB_2$–SiC studies between 1400 and 1600 °C [15, 16].

At 1800 °C and above, Layer III is replaced by Layer IV, the predominately $HfB_2$ layer. $SiO_2$ fills the entire porous $HfO_2$ layer at these temperatures. At 1800 °C the predominately $HfB_2$ layer contains both $SiO_2$ and Si–O–C inclusions. Layer IV forms two distinct layers at 1900 °C: $HfB_2$ with $SiO_2$ and $HfB_2$ with Si–O–C inclusions (nearest

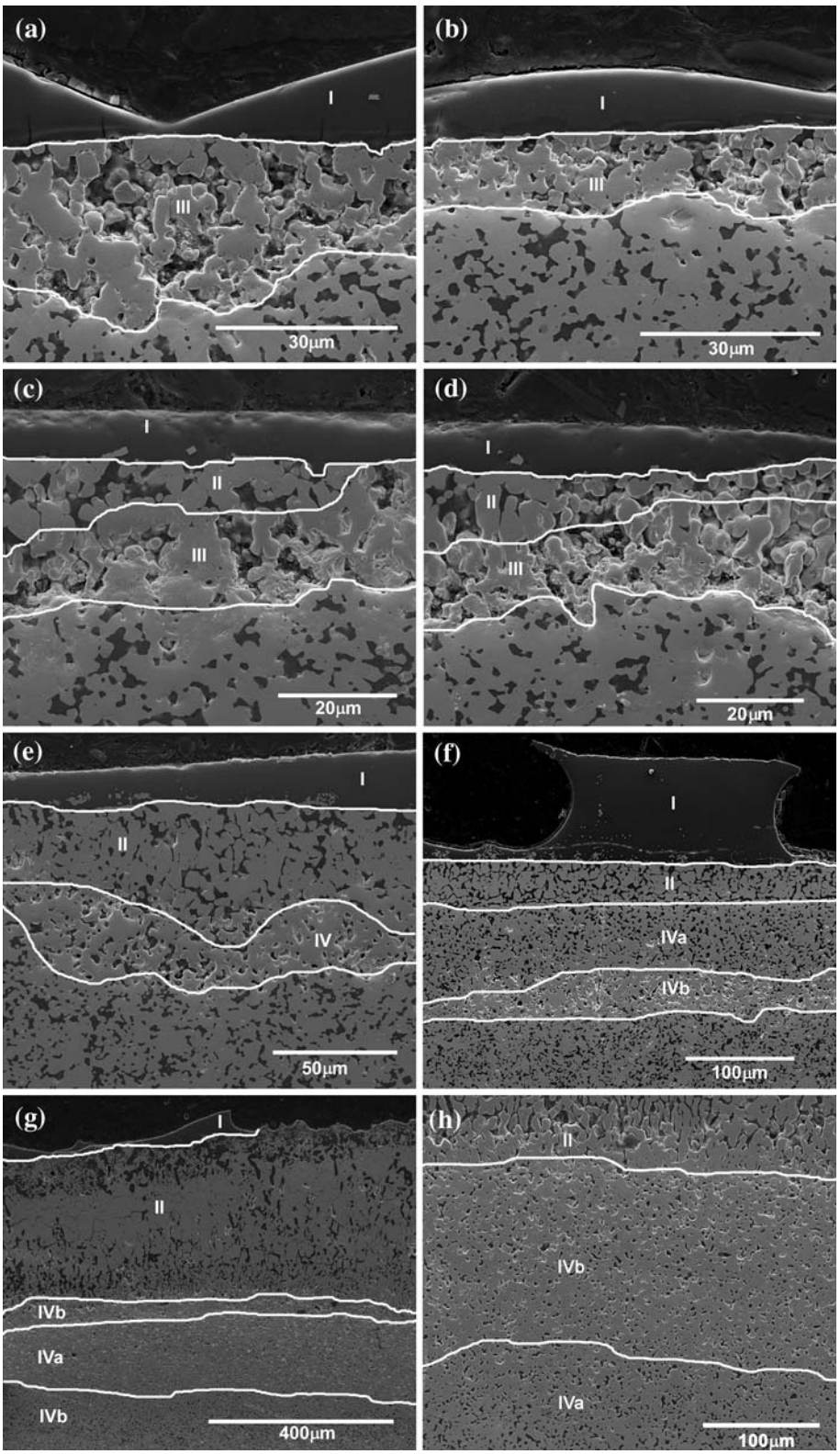


**Fig. 3** Series of SEM micrographs showing the progression of the oxide scale from **a** to **g** 1400, 1500, 1600, 1700, 1800, 1900, and 2000 °C, respectively. The *dark area* at the top of each image is the epoxy. The layers are defined as: (I) primarily $SiO_2$, (II) $SiO_2$ infiltrating $HfO_2$, (III) $HfO_2$ with inclusions of Si–O–C, and (IV) $HfB_2$ with Si–O–C and $SiO_2$. At 1900 and 2000 °C, two distinct layers form within layer (IV): $HfB_2$ with $SiO_2$ (IVa) and $HfB_2$ with Si–O–C (IVb). The boundaries of the layers are approximately outlined by the *white lines*. The scale thickness increases with temperature as shown by the changes in scale bars of the micrographs. **h** Magnified region of the 2000 °C sample (**g**) showing Layers II, IVb, and IVa

to the bulk). At 2000 °C Layer IV splits into three layers: a layer of $HfB_2$ with Si–O–C inclusions nearest to the surface, a layer of $HfB_2$ with $SiO_2$, and another layer of HfB2 with Si–O–C inclusions which comprises the entire center of the sample. At 2000 °C, the Si–O–C inclusions are almost entirely made up of C.

## Oxide scale morphology (arc jet heating)

Figure 4a is an SEM micrograph of the sample heated in the arc jet with a hold time of 3.6 min. The hold temperature seen on the face of the sample was between 1450 and 1570 °C. Figure 4b is a furnace-heated sample that was heated to 1500 °C in approximately 1 min by quickly moving the sample into the heated region of the furnace and held for 4 min. The oxide scale thickness for the furnace-heated sample is about half as thick (~7 μm compared to ~18 μm) as the arc jet heated sample. The furnace-heated sample that was held at 1500 °C for 1 h had an average scale thickness of 20 μm. The morphology of the layers for the arc jet and furnace-heated samples are the same and are mainly consists of porous $HfO_2$. There is minimal penetration of the $SiO_2$ (bold arrows in Fig. 4a) into the $HfO_2$, Layer II, and the predominately $HfO_2$, Layer III, with Si–C–O inclusions (thin arrows in Fig. 4a) are observed in both the samples. Following a particular grouping of SiC grains from the unaffected bulk to Layer II (the primarily porous $HfO_2$ layer) provides evidence that the Si–O–C inclusions are byproducts of SiC oxidation. The Si–O–C fill the same space once occupied by SiC and the $HfO_2$ maintains the structure of the original $HfB_2$ grains. These areas are boxed in Fig. 4b.

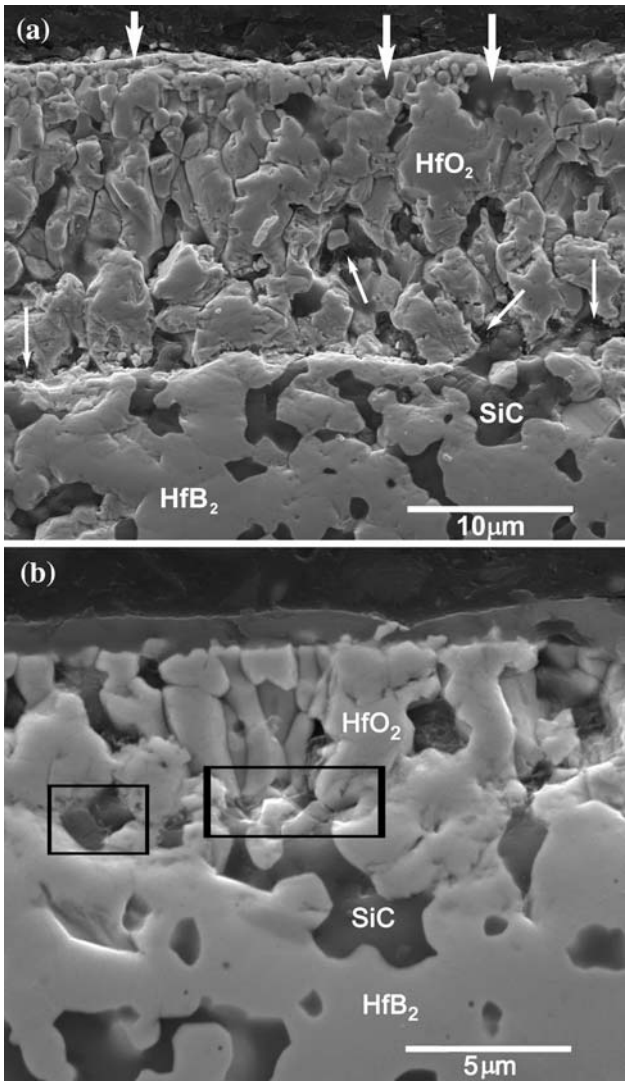


**Fig. 4** **a** SEM micrograph of the sample heated in the arc jet for 3.6 min at 260 MW/cm$^2$ (1450–1570 °C). The oxide scale consists of an $HfO_2$ matrix with $SiO_2$ in the top layer (examples indicated by *thick-lined arrow*) and Si–O–C inclusions (examples indicated by *thin-lined arrow*). **b** SEM micrograph of the sample heated in the furnace for 4 min at 1500 °C. The regions where SiC crosses from the unaffected bulk into Layer II are *boxed*. Note the magnification is ×2 that in (**a**)

## Oxide scale crystallography

In order to track the change in crystal structure of the oxide scale, samples heated to 1600, 1700, 1800, 1900, and 2000 °C were analyzed using XRD. After cooling, XRD scans were taken for each of the samples between 15° and 80° 2 $\theta$. Figure 5 shows a region of interest that highlights the phases present in the sample heated to 1800 °C. The major peaks can be attributed to monoclinic $HfO_2$ as expected. A small hump near 21° was observed in the XRD scans of all the samples before background subtraction which is an indicative of amorphous $SiO_2$ [17]. Peaks corresponding to tetragonal or cubic $HfO_2$ are found between 1700 and 2000 °C. The peaks for the tetragonal and cubic systems closely overlap and the determination between the two structures is difficult especially when the peaks are weak [18]. $HfSiO_4$ is present in samples heated to 1600 and 1800 °C. $HfSiO_4$ is the reaction product from the combination of $HfO_2$ and $SiO_2$. Calculated $HfO_2$–$SiO_2$ phase diagrams show that $HfSiO_4$ is stable up to ~1726 °C independent of the $SiO_2$ mole fraction [19]. However, there is limited thermodynamic data for the $HfO_2$–$SiO_2$ system and the experimental verification of the data mostly exists for temperatures below 1000 °C [20–22].

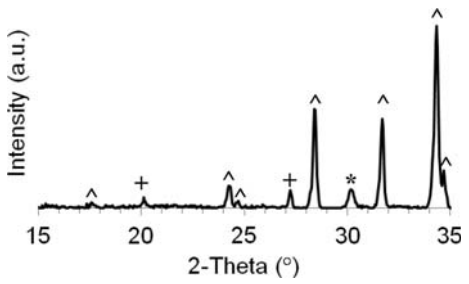


**Fig. 5** XRD after cooling of the sample oxidized in the $ZrO_2$ furnace at 1800 °C showing the monoclinic $HfO_2$ (^), tetragonal $HfO_2$ (*), and $HfSiO_4$ (+) phases

## Discussion

### Oxidation

Figure 2 shows the relationship between oxide scale thickness, weight gain per surface area, and percent weight gain of the sample versus the zirconia crucible. It is evident from these plots that these properties are all interrelated. The weight gain per surface area (Fig. 2a) increases by less than 1 mg/100 °C from 1400 to 1800 °C until it jumps more than 4 mg from 1800 to 1900 °C. This is the same temperature range that the $SiO_2$-rich glass begins to flow more readily as expected from its 1713 °C melting point and as evidenced by the increase in weight of the zirconia crucible (Fig. 2b). At 1900 °C, the scale thickness triples over the values found for the lower temperatures. This increase in scale thickness correlates with the doubling of weight gain at 1900 °C. The turning point for the change in the oxide scale structure is at 1800 °C. Below this temperature, the oxide scale consists of well-defined layers including an outer layer of $SiO_2$-rich glass on top of $HfO_2$ with some $SiO_2$ penetration into the porous $HfO_2$ grains and in the more inner portions partially oxidized SiC in the form of Si–O–C inclusions. At 1800 °C, the $SiO_2$ penetrating $HfO_2$ becomes the bulk of the scale and a layer of $HfB_2$ with partially oxidized SiC is observed.

$HfSiO_4$ is observed after heating the sample to 1800 °C (Fig. 5). The phase diagram of $HfSiO_4$ predicts its stability to be ~1726 °C and below. The $HfSiO_4$ phase may be formed upon heating or during cooling. Formation of $HfSiO_4$ occurs when silicon atoms diffuse into the $HfO_2$ crystal interstitially until the solubility limit is reached and has been shown to occur as low as 1100–1400 °C [20, 23]. This can occur in both Layer I between the $HfO_2$ crystals embedded in the $SiO_2$ matrix and Layer II when the $SiO_2$ fills the $HfO_2$ matrix. The formation of a crystalline solid from an amorphous glass may help limit oxygen penetration and therefore limits oxide scale growth; however, the $HfSiO_4$ phase is not continuous and there remains a substantial oxidation pathway through the amorphous $SiO_2$-rich glass. Additionally, there does not seem to be a correlation with the degree of oxidation and the presence of $HfSiO_2$.

The appearance of the tetragonal or cubic $HfO_2$ peaks in the XRD was observed for samples heated to 1700 °C and above making it likely that the phase transformation is monoclinic to tetragonal as expected from the Hf–O phase diagram [19, 20]. This phase transformation from monoclinic to tetragonal $HfO_2$ results in about 3.5% reduction in volume [4]. The monoclinic to tetragonal transition may be linked to the transition from equiaxed to columnar $HfO_2$ grains as reported previously around 1650 °C [4, 24]. The resulting volume decrease opens additional porosity in the $HfO_2$ matrix aiding the increased $SiO_2$ penetration observed at these temperatures and making the grains appear more elongated. In pure metal diborides, the transformation from monoclinic to tetragonal is shown to greatly enhance the oxidation of $HfB_2$ at ~1700 °C [25, 26]. However, the existence of $SiO_2$ appears to delay this effect since the total weight gain is less than 3% of the starting sample weight up to 1800 °C and doubles to 6% at 1900 °C.

A change in morphology may also be caused by a flow of borosilicate glass containing $HfO_2$. Studies involving $ZrB_2$–SiC [27, 28] discuss the convection of $ZrO_2$–$B_2O_3$–$SiO_2$ liquid driven to the surface by the volume change associated with oxidation The $ZrO_2$ then precipitates out of the liquid as it reaches the vicinity of the surface when the $B_2O_3$ evaporates. The metal oxide ($MeO_2$) phase is predicted to precipitate due to the fact that its solubility is higher in a borosilicate glass than in a pure silicate glass [27]. The phase diagrams of $HfO_2$–$SiO_2$ [19] and $ZrO_2$–$SiO_2$ [29] show that about 2 mol% $ZrO_2$ or $HfO_2$ may be dissolved in the pure $SiO_2$ liquid at the eutectic point (1687 °C for $ZrO_2$–$SiO_2$ and around 1450 °C for $HfO_2$–$SiO_2$), while the amount of dissolvable $MeO_2$ increases with temperature. At 2000 °C approximately 40 mol% $HfO_2$ or 11 mol% $ZrO_2$ would be soluble in $SiO_2$ before precipitating as a tetragonal crystal. Upon cooling, the excess $HfO_2$ would precipitate in the $SiO_2$ layer. The flow of $MeO_2$–$B_2O_3$–$SiO_2$ liquid is predicted to leave an underlying columnar $MeO_2$ layer and smaller equiaxed oxide particles near or in the $SiO_2$ layer. At 1400 and 1500 °C less than 25 distinct $HfO_2$ grains are observed in the $SiO_2$ layer (Layer I) in the cross section of the samples. These grains are identified by their contrast difference with $SiO_2$ and confirmed with EDS. At 1600 °C the population of 1–2-μm $HfO_2$ grains within the $SiO_2$ layer increases (Fig. 3) and at 1900 and 2000 °C the grains exist throughout the $SiO_2$ scale. A systematic oxidation study of $ZrB_2$–SiC between 1600 and 1900 °C with hold times of 1 h [28] showed similar oxide scales as observed in this study. At 1600 °C, a $SiO_2$ layer covers a $ZrO_2$ layer whose pores are filled with $SiO_2$. A SiC-depleted region is not observed until 1700 °C, while oriented growth of $ZrO_2$ is observed at 1800 °C. At 1800 °C, the SiC-depleted region is said to contain "minor" amounts of Si, but there is no discussion as to whether this is in the form of $SiO_2$, SiC, or something else. At 1900 °C, a SiC-depleted layer is observed in $ZrB_2$ similar to Layer IV found for the oxidation of $HfB_2$–SiC at 1800 °C and higher. Since the monoclinic to tetragonal transformation temperature of $ZrO_2$ is between 1000 and 1150 °C, the structural change of $ZrO_2$ from equiaxed to columnar between 1700 and 1800 °C would not be expected to be caused by a phase transformation. Therefore, the columnar growth habit in

both $HfB_2$–SiC and $ZrB_2$–SiC are from the interaction of the $MeO_2$ with the borosilicate glass and its convection.

Between 1400 and 2000 °C in the $HfB_2$–SiC system there are four competing factors contributing to oxidation: (1) the formation of $HfO_2$, (2) the formation and stability of the $SiO_2$ scale, (3) the presence of $HfSiO_4$, and (4) the transition in morphology and increase in porosity caused by a phase transformation and/or convection of $HfO_2$–$B_2O_3$–$SiO_2$ liquid. From the observations, it seems as though the stability of the $SiO_2$ layer plays the most important role in oxidation protection with the apparent opening of porosity playing a supporting role. Methods that have been proposed to increase oxidation resistance include engineering the glassy phase by either inducing phase separations by the addition of Group IV–VI transition metals [11] or by the addition of different combinations of $Na_2O$, $Al_2O_3$, and/or $B_2O_3$ to incorporate additional $HfO_2$ [9, 30]. However, decreasing the solubility of $HfO_2$ may aid in slowing the transport of $HfO_2$ from the porous oxide scale to the $SiO_2$ amorphous scale and thereby suppresses the formation of additional porosity. The incorporation of $TaSi_2$ has been shown to increase oxidation resistance of $ZrB_2$–SiC ceramics up to 1600 °C, but has conflicting results at higher temperatures [6, 31]. Additionally, stabilizing agents may be alloyed within the UHTC to delay or halt the monoclinic to tetragonal phase transformations of the $HfO_2$.

### Comparison between testing variations

There is no significant difference between samples heated in the $MoSi_2$ and $ZrO_2$ furnaces. Comparisons of the weight gain and morphology (not shown) of the samples heated to 1600 °C in both furnaces show the same results.

In arc jet testing one might expect a catalytic atom recombination effect due to the presence of dissociated O and N present in the heating plasma of the arc jet (and also at the leading edges in hypersonic flight); however, recombination effects at the surface of $ZrB_2$ and $HfB_2$ and particularly their oxides have been shown to be negligible [32, 33]. Additionally, the stagnation pressure inside the arc jet may be less than 1 atm (in this test stagnation pressure was 0.1 atm) which can influence the active to passive transitions in the oxidation of the samples. This is especially true with the oxidation of SiC. When active oxidation of SiC occurs the protective $SiO_2$ layer can be removed as gaseous SiO. This active oxidation may account for the very thin (0–0.8 μm) outer $SiO_2$ layer observed on the arc jet heated sample when compared to the ~0.5–5-μm $SiO_2$ layer formed on the furnace-heated sample. This lack of outer $SiO_2$ may lead to accelerated oxidation and the longer oxide scale observed for the arc jet heated sample (~18 μm) compared to the sample that was furnace heated for 4 min (~7 μm). Rezaie et al. [34] have shown that $ZrB_2$–SiC heated to 1500 °C in a lower oxygen partial pressure has a thinner outer $SiO_2$ layer and a thicker overall oxide scale when compared to the same sample heated in air. Some $SiO_2$ may also be lost due to the shear forces of the plasma. These effects would become increasing important with increases in temperature as the $SiO_2$ becomes more fluid. This effect does not change the morphology and chemistry of the oxide scale near 1500 °C as the arc jet heated sample and the furnace-heated samples held at 4 min and 1 h all consists of a $SiO_2$ outer layer (Layer I) and a porous $HfO_2$ layer with Si–O–C inclusions (Layer II).

Arc jet tests published by Gasch et al. [11] with a steady-state temperature between 1690 and 1750 °C for a total exposure time of 20 min can be used as a comparison for the high-temperature tests (>1600 °C) in this study. As in our 1600 and 1700 °C furnace-heated samples, the oxide scale was described to consist mainly of a porous $HfO_2$ layer. They also report an $HfB_2$ layer with SiC removed (there is no mention of Si–O–C inclusions in the description of the arc jet sample). The total oxide scale thickness of the arc jet heated sample was 72 μm when compared to the 39-μm total oxide scale observed in the 1700 °C furnace-heated sample of this study that was held at temperature for a longer time. From our 1500 °C data and the literature data, one can conclude that the furnace tests can reproduce the basic microstructures of the oxidized $HfB_2$–SiC found in arc jet tests, but the total scale thickness is limited by a thicker protective $SiO_2$ outer layer in the furnace tests.

## Conclusion

Samples were heated in air from 1400 to 2000 °C using a $MoSi_2$ and $ZrO_2$ furnace. These samples were shown to develop four layers over this temperature range. Below 1800 °C, the oxide scale consists of three layers: Layer I, a protective $SiO_2$; Layer II, $SiO_2$ infiltrating into porous $HfO_2$; and Layer III, predominantly porous $HfO_2$. At 1800 °C and above, the oxide layer consists of three layers: Layer I, a protective $SiO_2$; Layer II, $SiO_2$ infiltrating into porous $HfO_2$; and Layer IV, predominately $HfB_2$. Regions of the predominately $HfO_2$ and $HfB_2$ layers both contained inclusions of Si–O–C indicating partially oxidized SiC. Up to 2000 °C, the critical factors influencing oxidation were shown to be the flow of $SiO_2$ glass and an apparent increase in porosity of the $HfO_2$ oxide scale. The outer oxide scale must be protective against oxygen penetration and as shown by the comparison of furnace-heated samples to arc jet heated samples must be resistant to active oxidation. In order to increase the working times at elevated temperatures

(>1800 °C) it is necessary to develop a more robust protective glassy scale through the use of additives with $SiO_2$ to increase the viscosity or melting temperature or to stabilize the $HfO_2$ crystalline phase.

**Acknowledgements** This study was supported in part by the United States Air Force Contract # FA8650-04-D-5233 with project manager Michael Cinibulk. We acknowledge NASA-SCAP for their critical financial support of the arc jet operational capability at Ames. And we would like to thank Sylvia Johnson and Matthew Gasch at NASA Ames for their assistance in performing the arc jet testing.

## References

1. Monteverde F, Scatteia L (2007) J Am Ceram Soc 90(4):130
2. Fenter JR (1971) SAMPE Quart 2(3):1
3. Fahrenholtz WG, Hilmas GE, Talmy IG, Zaykoski A (2007) J Am Ceram Soc 90(5):1347
4. Kaufman L, Clougherty EV, Berkowitz-Mattuck JB (1967) Trans Metall Soc AIME 239:458
5. Hinze JW, Tripp WC, Graham HC (1975) J Electrochem Soc 122(9):1249
6. Opila E, Levine S, Lorincz J (2004) J Mater Sci 39:5969. doi:10.1023/B:JMSC.0000041693.32531.d1
7. Lide DR (1996) CRC handbook of chemistry and physics, 77th edn. CRC Press Inc, Boca Raton (Sect. 4)
8. Clougherty EV, Pober RL, Kaufman L (1968) Trans Metall Soc AIME 242:1077
9. Lespade P, Richet N, Goursat P (2007) Acta Astronautica 60:858
10. Monteverde F (2005) Corr Sci 47:2020
11. Gasch M, Ellerby D, Irby S, Beckman S, Gusman M, Johnson S (2004) J Mater Sci 39(19):5925. doi:10.1023/B:JMSC.0000041689.90456.af
12. Zhang X, Weng L, Han J, Meng S, Han W (2009) Int J App Ceram Technol 6(2):134
13. Licheri R, Orrù R, Musa C, Locci AM, Cao G (2009) J Alloys Comp 478(1–2):572
14. Carney CM, Moglivesky P, Parthasarathy TA (2009) J Am Ceram Soc. doi:10.1111/j.1551-2916.2009.03134.x
15. Monteverde F, Scatteia L (2007) J Am Ceram Soc 90(4):1130
16. Monteverde F (2006) App Phys A 82:329
17. Liu K, Feng Q, Yang Y, Zhang G, Ou L, Lu Y (2007) J Non-Cryst Solids 353:1534
18. Srinivasan R, De Angelis RJ, Ice G, Davis BH (1991) J Mater Res 6(6):1287
19. Shin D, Arroyave R, Liu Z-K (2006) CALPHAD 30:375
20. Ushakov SV, Navrotsky A, Yang Y, Stemmer S, Kukli K, Ritali M et al (2004) Phys Stat Sol 241(10):2268
21. Lee J-H (2005) Thin Sol Films 472:317
22. Bongiorno A, Först CJ, Kalia RK, Li J, Marschall J, Nakano A et al (2006) Mater Res Soc Bull 31:410
23. Nguyen QGN, Opila EJ, Robinson RC (2004) J Electrochem Soc 151(10):B558
24. Berkowitz-Mattuck JB (1966) J Electrochem Soc 113(9):908
25. Parthasarathy TA, Rapp RA, Opeka M, Kerans RJ (2009) J Am Ceram Soc 92(5):1079
26. Talmy IG, Zaykoski JA, Opeka MM, Dallik S (2001) In: Opila EJ, McNallan MJ, Shores DA, Shifler DA (eds) High-temperature corrosion and materials chemistry III. The Electrochemical Society, Pennington, p 144
27. Karldottir SN, Halloran JW (2008) J Am Ceram Soc 91(1):272
28. Zhang X-H, Hu P, Han J-C (2008) J Mater Res 23(7):1961
29. Butterman WC, Foster WR (1967) Am Min 52(5–6):880
30. Davis LL, Li L, Darab JG, Li H, Strachan D (1999) Mater Res Soc Symp Proc 556:313
31. Opeka MM, Talmy IG, Zaykoski JA (2004) J Mater Sci 39:5887. doi:10.1023/B:JMSC.0000041686.21788.77
32. Marschall J, Chamberlain A, Crunkleton D, Rogers B (2004) J Spacecr Rocket 41(4):576
33. Scatteia L, Borrelli R, Cosentino G, Bêche E, Sans J-L, Balat-Pichelin M (2006) J Spacecr Rocket 43(5):1004
34. Rezaie A, Fahrenholtz WG, Hilmas GE (2006) J Am Ceram Soc 89(10):3240